

A Spatially Consistent Geometric D2D Small-Scale Fading Model for Multiple Frequencies

Stephan Jaeckel*, Leszek Raschkowski*, Frank Burkhardt[†] and Lars Thiele*

* Fraunhofer Heinrich Hertz Institute, Berlin, Germany, stephan.jaeckel@hhi.fraunhofer.de

[†] Fraunhofer Institute for Integrated Circuits, Erlangen, Germany

Abstract—The 3GPP new radio (NR) channel model introduced spatial consistency and a correlation model for multiple frequencies. Future extensions of this model will incorporate mobility at both ends of the link. These features are essential for many emerging wireless technologies in the 5G era. However, the existing small-scale-fading (SSF) model does not integrate these features coherently. To solve this problem, we propose a new SSF model that seamlessly integrates with the remaining NR model and allows the simultaneous simulation of all three features. We demonstrate this integration by showing that the output of the new SSF model agrees well with large-scale fading (LSF) parameter distributions provided by 3GPP. This enables the simulation of new wireless technology proposals that were difficult to realize with existing geometry-based stochastic channel models (GSCMs).

I. INTRODUCTION

GSCMs are a well-established tool to model wireless propagation channels. They consist of two main components: a stochastic part that generates a random propagation environment, and a deterministic part that lets transmitters (TXs) and receivers (RXs) interact with this environment. To predict the wireless system performance, the random environment must fulfill certain statistical properties which are determined by measurements. These properties are generated by the so-called LSF model. A subsequent SSF model generates individual multipath components (MPCs) for each mobile terminal (MT). GSCMs became widely used by the 3rd generation partnership project (3GPP) which required standardized models to evaluate new technology proposals. This was provided by the spatial channel model (SCM) in 2003 [1]. Since then, this model has undergone many iterations to support new features of the fast evolving wireless world. However, the SSF model has not been significantly enhanced which leads to incompatibilities with some newly introduced features of the NR model [2].

The NR model proposes to correlate all random variables that determine the powers, delays and angles of the MPCs. This so-called spatial consistency solves one major drawback of previous GSCMs, namely the lack of realistic correlation in multi-user wireless channels. An efficient way to do this is by utilizing the sum-of-sinusoids (SOS) method in [3]. However, to be truly consistent, any function that modifies these random variables must be continuous. For example, the delay generation in [2] requires to sort the delays ([2], eq. 7.5-2). Sorting is not a continuous function since it changes the order of the MPCs depending on their delay. As a result, the channel coefficients show sudden “jumps” when plotting

the phase over time on a continuous MT trajectory. The same happens for the scaling with the maximum path power when generating the arrival and departure angles ([2], eqs. 7.5-9 and 7.5-14), the positive or negative sign in the angles (eq. 7.5-16), and the random coupling of rays within a multipath cluster. All these operations break the spatial consistency. The NR model also introduces an alternative channel generation method to support multi-frequency simulations, e.g., for combined sub-6-GHz and mm-wave channels. The rationale is that, for a given environment, a MT “sees” the same propagation paths (the same clusters), but with different power. Hence, delays and angles are kept fixed and path-powers are modified to account for the different Ricean K-factor (KF), delay spread (DS) and angular spreads (ASs) at different frequencies. However, the proposed method does not ensure that the output of the SSF model (the channel coefficients) is consistent with the input (the LSF parameters). Lastly, emerging wireless technologies increasingly require the support for device-to-device (D2D) communications, such as in vehicular networks, air-to-ground communications, industrial communications, or communication scenarios involving satellites in low-earth orbit. All of these use cases require that both ends of the link are mobile.

This paper addresses these issues by proposing a new SSF model which replaces steps 5, 6, and 7 of the 3GPP NR channel generation procedure (see [2], pp. 32). The method is introduced in Section II. Numeric results are presented and discussed in Section III. An open-source implementation is available as part of the quasi deterministic radio channel generator (QuaDRiGa) [4].

II. A NEW SMALL-SCALE FADING MODEL

The communication model consists of multiple TXs and multiple RXs. Their locations are given in three-dimensional (3-D) metric Cartesian coordinates as (x_t, y_t, z_t) and (x_r, y_r, z_r) , respectively. A transmitted signal is reflected and scattered by objects in the environment such that multiple copies of that signal are received by the RX. Each signal *path* consists of a departure direction at the TX, a first-bounce scatterer (FBS), a last-bounce scatterer (LBS), and an arrival direction at the RX. Departure and arrival directions are given in geographic coordinates consisting of an azimuth angle ϕ and an elevation angle θ ¹. The formulation of the path

¹ ϕ is defined in mathematic sense, *i.e.*, seen from above, a value of 0 points to the east and the angles increase counter-clockwise. θ is oriented relative to the horizontal plane. Positive angles point upwards.

generation procedure is done for the dual-mobility case, where both ends of the link can be mobile. For any two channel realizations, the TX can be in a different position with d_t describing the distance between the two positions. Likewise, the RX can be displaced by a distance d_r . Single-mobility is a special case where either d_t or d_r is zero. All random variables that determine the positions of the non-line of sight (NLOS) scatterers are spatially correlated, *i.e.*, they depend on the positions of the TX and the RX [3].

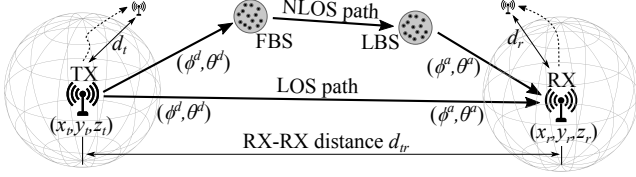


Fig. 1. Illustration of the communication model

a) *Initial Delays and Angles:* Initial delays for the NLOS paths are drawn randomly from a single-sided exponential distribution with unit mean and unit variance as

$$\tilde{\tau}_l = -\ln \{X_l^\tau(x_t, y_t, z_t, x_r, y_r, z_r)\}, \quad (1)$$

where the index l denotes the path number and $X_l^\tau \sim \mathcal{U}(0, 1)$ is a spatially correlated uniformly distributed random variable having values between 0 and 1. The line of sight (LOS) delay, *i.e.*, the delay of the first path, is set to 0. The initial delays are not scaled by the DS nor are the angles scaled by the AS. This approach is different compared to the NR model [2] which includes the spreads already in the initial values. The autocorrelation function (ACF) of X_l^τ is a combination of a Gaussian and an exponential ACF

$$\rho_\tau(d) = \begin{cases} \exp\left(-\frac{d^2}{d_\lambda^2}\right), & \text{for } d < d_\lambda; \\ \exp\left(-\frac{d}{d_\lambda}\right), & \text{for } d \geq d_\lambda, \end{cases} \quad (2)$$

where d is the distance between two MTs positions and d_λ is the decorrelation distance, *i.e.*, the distance at which the correlation falls below $e^{-1} \approx 0.37$ [5]. The combined ACF produces a higher correlation between delays of closely spaced MTs. It was found that this is more realistic compared to an exponential ACF where the delays may vary significantly even when MTs move only a few centimeters. If TX and RX are swapped, path delays must be identical. This is known as channel reciprocity and can be modeled by generating random variables X_l^τ in (1) as

$$X_l^\tau(x_t, y_t, z_t, x_r, y_r, z_r) = \frac{1}{2} \operatorname{erfc} \left(-\frac{\tilde{X}_l^\tau(x_t, y_t, z_t) + \tilde{X}_l^\tau(x_r, y_r, z_r)}{2 \cdot \sqrt{\rho_\tau(d_{tr}) + 1}} \right), \quad (3)$$

where the complementary error function maps the spatially correlated normal distributed random variables \tilde{X}_l^τ to a uniform distribution required by (1). The scaling with $\sqrt{\rho_\tau(d_{tr}) + 1}$ ensures that the variance of the random process does not change for small TX-RX distances. As for the

DS, the initial values for the angles are generated spatially consistent having the same ACF and decorrelation distance. The NR model [2] proposes to obtain the azimuth angles from a wrapped Gaussian distribution, the elevation angles from a wrapped Laplacian distribution, and the path power from a single slope exponential power delay profile (PDP). However, this leads to large angle offsets when the powers are small and the AS is large. Due to the wrapping operation, the achievable AS is limited. In order to have a larger range of possible angular spreads, we propose to draw all initial NLOS angles from a uniform distribution and apply the correct AS by a subsequent scaling operation. If TX and RX change places, channel reciprocity requires that the departure angles at the TX become the arrival angles at the RX and vice-versa. This effect is captured by generating two independent spatially correlated normal distributed random variables \tilde{X}_l^A and \tilde{X}_l^B and combining them to

$$\tilde{\phi}_l^d(x_t, y_t, z_t, x_r, y_r, z_r) = \frac{\pi}{2} \operatorname{erfc} \left(-\frac{\tilde{X}_l^A(x_t, y_t, z_t) + \tilde{X}_l^B(x_r, y_r, z_r)}{2} \right) - \frac{\pi}{2}, \quad (4)$$

$$\tilde{\phi}_l^a(x_t, y_t, z_t, x_r, y_r, z_r) = \frac{\pi}{2} \operatorname{erfc} \left(-\frac{\tilde{X}_l^B(x_t, y_t, z_t) + \tilde{X}_l^A(x_r, y_r, z_r)}{2} \right) - \frac{\pi}{2}, \quad (5)$$

where the complementary error function maps the resulting values to $\mathcal{U}(-\frac{\pi}{2}, \frac{\pi}{2})$. The same procedure is repeated for the initial elevation angles $\tilde{\theta}_l^d$ and $\tilde{\theta}_l^a$. The initial angles for the LOS path are set to 0.

b) *Initial Path Powers:* The initial delays $\tilde{\tau}_l$ and the initial angles $\tilde{\phi}_l^d$, $\tilde{\phi}_l^a$, $\tilde{\theta}_l^d$, and $\tilde{\theta}_l^a$ are assumed to be frequency-independent, *i.e.*, a MT sees the same scattering clusters at different frequencies and therefore, the same angles and delays are used. However, DS and AS are generally frequency-dependant [6]. For example, the DS at a carrier frequency of 10 GHz is generally shorter than at 2 GHz. The NR model [2] proposes an optional method which can adjust the path powers such that different delay and angular spreads can be achieved. The powers are calculated as

$$\tilde{P}_{l,f} = \exp \{ -\tilde{\tau}_l g_f^{\text{DS}} \} \cdot \exp \left\{ -(\tilde{\phi}_l^d)^2 g_f^{\text{ASD}} \right\} \cdot \exp \left\{ -(\tilde{\phi}_l^a)^2 g_f^{\text{ASA}} \right\} \cdot \exp \left\{ -|\tilde{\theta}_l^d| g_f^{\text{ESD}} \right\} \cdot \exp \left\{ -|\tilde{\theta}_l^a| g_f^{\text{ESA}} \right\}, \quad (6)$$

where the index f refers to the $f = 1 \dots F$ carrier frequencies. The scaling coefficients g_f^{DS} , g_f^{ASD} , g_f^{ASA} , g_f^{ESD} , and g_f^{ESA} need to be calculated such that the frequency-dependent differences in the spreads are reflected in the powers. For single-frequency simulations, the NR model [2] uses the delay distribution proportionality factor r_τ to shape the PDP. r_τ typically has values in between 1.7 and 3.8 and it follows from ([2], eq. 7.5-5) that $g_f^{\text{DS}} = r_\tau - 1$. However, for the multi-frequency simulations, there might be a different DS for each frequency. In this case, g_f^{DS} is a function of the frequency and so is r_τ .

Hence, it is not possible to fix r_τ to a given value. Instead, we propose to calculate g_f^{DS} by fitting a logarithmic function to the delays (1) and powers $\tilde{P}_{l,f} = \exp\{-\tilde{\tau}_l g_f^{\text{DS}}\}$ as

$$g_f^{\text{DS}} = -1.5 \cdot \ln \{1.2 \cdot \overline{\text{DS}}_f - 0.15\}. \quad (7)$$

The DS values must be normalized to obtain a value $\overline{\text{DS}}_f$ for each frequency.

$$\overline{\text{DS}}_f^* = \frac{\text{DS}_f}{\max_{\forall f} \{\text{DS}_f\} + \min_{\forall f} \{\text{DS}_f\}}$$

$$\overline{\text{DS}}_f = \max \left\{ \min \left(\overline{\text{DS}}_f^*, 0.15 \right), 0.85 \right\} \quad (8)$$

If there is no frequency dependency of the DS, then g_f^{DS} will have a value of 1.2 which corresponds to $r_\tau = 2.2$. A similar mapping is done for the AS. The initial angles (??) are uniformly distributed having values in between $-\pi/2$ and $\pi/2$. As for the DS, the scaling coefficients for the angular spreads g_f^{ASD} , g_f^{ASA} , g_f^{ESD} , and g_f^{ESA} are obtained by

$$g_f^{\text{ASD/A}} = -2.2 \cdot \ln \{1.5 \cdot \overline{\text{AS}}_f - 0.35\} \quad (9)$$

$$g_f^{\text{ESD/A}} = -3.4 \cdot \ln \{1.2 \cdot \overline{\text{AS}}_f - 0.1\} \quad (10)$$

$$\overline{\text{AS}}_f = \min \left(\frac{0.75 \cdot \text{AS}_f}{\max_{\forall f} \{\text{AS}_f\}}, 0.25 \right). \quad (11)$$

If there is no frequency dependency, then $g_f^{\text{ASD/A}}$ will have a value of 0.56 which corresponds to an initial azimuth spread of 42° . The scaling coefficient $g_f^{\text{ESD/A}}$ will have a value of 0.76 which corresponds to an initial elevation spread of 44° . Both can be scaled down to 14° at a different frequency.

c) *Applying K-Factor, Delay Spread and Angle Spreads:*

The initial delays $\tilde{\tau}_l$ and powers $\tilde{P}_{l,f}$ are chosen such that the DS can have values between 0.15 and 0.85 seconds. The cluster angles $\tilde{\phi}_l^d$, $\tilde{\phi}_l^a$, $\tilde{\theta}_l^d$, $\tilde{\theta}_l^a$ are initialized such that the initial ASs can have values between 14° and 42° . Hence, the initial cluster powers already take the frequency-dependent differences for the DS and ASs into account. Next, the absolute values of the KF, the DS and the four ASs are applied.

The KF is the ratio of the power of the direct path to the sum-power of all other paths. It is applied by scaling the power of the first path and normalizing the PDP to unit power. This is done independently for each frequency.

$$\tilde{P}_{1,f} = \text{KF}_f \cdot \sum_{l=2}^L \tilde{P}_{l,f} \quad P_{l,f} = \tilde{P}_{l,f} / \sum_{l=1}^L \tilde{P}_{l,f} \quad (12)$$

The DS measures how the multipath power is spread out over time. Given the cluster-powers $P_{l,f}$ from (12) and the initial delays $\tilde{\tau}_l$ from (1), the initial DS is calculated as

$$\widetilde{\text{DS}}_f = \sqrt{\frac{1}{P_f} \cdot \sum_{l=1}^L P_{l,f} \cdot (\tilde{\tau}_l)^2 - \left(\frac{1}{P_f} \cdot \sum_{l=1}^L P_{l,f} \cdot \tilde{\tau}_l \right)^2}, \quad (13)$$

where P_f is the sum-power of all clusters at frequency f . The values of $\widetilde{\text{DS}}_f$ are frequency-dependent due to the scaling of the path-powers in (6), but do not contain the correct DS values from the LSF model. Hence, the delays need to be scaled such

that the correct DS can be calculated from the generated path-delays and path-powers. This is done by

$$\tau_l = \tilde{\tau}_l \cdot \frac{1}{F} \cdot \sum_{f=1}^F \frac{\text{DS}_f}{\widetilde{\text{DS}}_f}. \quad (14)$$

The AS measures how the multipath power is spread out in the spatial domain. The AS is ambiguous since the angles are distributed on a sphere and the resulting value depends on the reference angle, *i.e.*, the definition of where 0° is. A linear shift of the angles $\phi_l + \Delta_\phi$ leads to the AS being a function of Δ_ϕ . We therefore normalize the angles such that the combined power-angular spectrum (PAS) of all paths and sub-paths points to $\theta = \phi = 0$. The AS is calculated by

$$\Delta_{\phi_f} = \arg \left(\sum_{l=1}^L \exp \{j \tilde{\phi}_l\} \cdot P_{l,f} \right), \quad (15)$$

$$\hat{\phi}_{l,f} = \arg \exp \left\{ j \left(\tilde{\phi}_l - \Delta_{\phi_f} \right) \right\} \quad (16)$$

$$\widetilde{\text{AS}}_f = \sqrt{\frac{1}{P_f} \cdot \sum_{l=1}^L P_{l,f} \cdot (\hat{\phi}_{l,f})^2 - \left(\frac{1}{P_f} \cdot \sum_{l=1}^L P_{l,f} \cdot \hat{\phi}_{l,f} \right)^2}. \quad (17)$$

With AS_f being the initial AS from the LSF model, the initial angles $\tilde{\phi}_l$ are scaled to

$$\phi_l = \arg \exp \left(j \cdot \tilde{\phi}_l \cdot s \right), \quad s = \frac{1}{F} \cdot \sum_{f=1}^F \frac{\text{AS}_f}{\widetilde{\text{AS}}_f},$$

$$s < \begin{cases} 3.0, & \text{for azimuth angles;} \\ 1.5, & \text{for elevation angles.} \end{cases} \quad (18)$$

The $\arg \exp$ function wraps the angles around the unit circle. The scaling coefficient s is limited to a maximum value of 3 for the scaling of the azimuth angles and 1.5 for the elevation angles. This is motivated by the distribution of the initial angles in (??). More power is assigned to the angles having values close to 0 than to those having values close to $\pm \frac{\pi}{2}$. For this reason, $s = 3$ achieves the maximum azimuth AS of around 80° and $s = 1.5$ achieves the maximum elevation AS of around 45° . Larger values of s tend to decrease the AS again due to the wrapping around the unit circle.

d) *LOS angles:* The last step is to apply the direction of the LOS path. The initial values of the LOS angles $\tilde{\phi}_1^d$, $\tilde{\phi}_1^a$, $\tilde{\theta}_1^d$, and $\tilde{\theta}_1^a$ were set to 0. However, the correct angles need to take the positions of the TX and the RX into account. The LOS angles are

$$\phi_1^d = \arctan_2 \{y_r - y_t, x_r - x_t\}, \quad (19)$$

$$\phi_1^a = \phi_1^d + \pi \quad (20)$$

$$\theta_1^d = \arctan_2 \{z_r - z_t, d_{2d}\}, \quad (21)$$

$$\theta_1^a = -\theta_1^d, \quad (22)$$

$$d_{2d} = \sqrt{(x_r - x_t)^2 + (y_r - y_t)^2} \quad (23)$$

where $\arctan_2(y, x)$ is the four quadrant inverse tangent of the elements y and x having values between $-\pi$ and π . Those angles are applied by two 3-D rotations in Cartesian

coordinates, one for the TX and one for the RX. The operations are identical. The NLOS departure and arrival angles from the previous calculation are converted to Cartesian coordinates by

$$\mathbf{c}_l = \begin{pmatrix} \cos \theta_l \cdot \cos \phi_l \\ \cos \theta_l \cdot \sin \phi_l \\ \sin \theta_l \end{pmatrix}. \quad (24)$$

Then, a rotation matrix is constructed from the LOS angles. This matrix is a combined rotation around the y -axis followed by a rotation around the z -axis in Cartesian coordinates. It is applied by

$$\hat{\mathbf{c}}_l = \begin{pmatrix} \cos \theta_1 \cdot \cos \phi_1 & -\sin \phi_1 & -\sin \theta_1 \cdot \cos \phi_1 \\ \cos \theta_1 \cdot \sin \phi_1 & \cos \phi_1 & -\sin \theta_1 \cdot \sin \phi_1 \\ \sin \theta_1 & 0 & \cos \theta_1 \end{pmatrix} \cdot \mathbf{c}_l. \quad (25)$$

The final angles are then obtained by converting $\hat{\mathbf{c}}_l$ back to spherical coordinates.

$$\phi_l = \arctan_2 \{ \hat{c}_{l,y}, \hat{c}_{l,x} \} \quad (26)$$

$$\theta_l = \arctan_2 \left\{ \hat{c}_{l,z}, \sqrt{\hat{c}_{l,x}^2 + \hat{c}_{l,y}^2} \right\} \quad (27)$$

III. NUMERIC EVALUATIONS AND DISCUSSION

The aim of this section is to show how well the propagation parameters from 3GPP-NR model can be mapped to delays, angles and powers of individual MPCs in a wireless channel. For the evaluation of the new SSF model we used QuaDRiGa version 2.2 which implements both, the 3GPP-NR baseline model and the new SSF model presented in this paper.

The new SSF model was evaluated for the urban-microcell (UMi) scenario. The model parameters for LOS and NLOS propagation conditions are given by [2], table 7.5-6. Evaluations were done for three different carrier frequencies: 1 GHz, 6 GHz, and 60 GHz. A single base station (BS) was placed at a height of 10 m and 500 MTs were randomly placed within a 200 m radius around the BS. The MT height was set to 1.5 m. Both, the BS and the MTs used isotropic antennas to remove the influence of the antenna patterns from the results. The evaluations were done as follows:

- 1) Each MT gets assigned a specific value of the DS, the four ASs and the KF as described in [2], page 31, step 4. These values are the input to the new SSF model.
- 2) The input parameters get mapped to delays, angles and path-powers as described in Section II of this paper.
- 3) The delay and angular spreads are calculated from the generated MPCs using (13) and (17).

As a result, we obtain the distribution of the input values from step 1 and the distribution of the output values from step 3. Ideally, these distributions are identical, i.e., the SSF model maps LSF parameters exactly. Results are shown in Fig. 3. The figure consists of 10 plots, each showing 6 empiric cumulative distribution functions (CDFs). The black curves show the results for 60 GHz, the red curves for 6 GHz and the blue curves for 1 GHz. Plots on the left-hand side are for LOS propagation and plots on the right-hand side are for NLOS propagation. The thin, dashed curves were obtained

from the input values, i.e., the distributions given by [2], table 7.5-6. The thick, solid curves were obtained from the output of the SSF model. In addition, median values for the input and output are listed in the bottom right of each figure.

Except for the elevation spread of departure (ESD), all parameters are frequency-dependent where the values decrease with increasing frequency, i.e., the DS is shorter at 60 GHz compared to 1 GHz. A generally good match between input and output of the new SSF model can be achieved for most of the parameters. The DS can be precisely mapped to path-delays and path-powers with ns-accuracy despite the fact that identical delay are used for all frequencies. The same holds true for the azimuth spread of departure (ASD) and the elevation spread of arrival (ESA) which is accurate within 1° . However, there are some significant offsets for the azimuth spread of arrival (ASA) and the ESD.

Mapping the ASs of the LSF model to scattering clusters fails when the azimuth angles have values outside the $-\pi$ to π range or elevation angles exceed the $-\frac{\pi}{2}$ to $\frac{\pi}{2}$ range. This fact was also acknowledged by the 3GPP-NR model [2] where the azimuth AS is capped at 104° and the elevation AS is capped at 52° . However, this does not consider the influence of the KF which limits the AS even further when more power is allocated to the LOS path. For example, with a KF of 10 dB the maximum azimuth spread is 57° , provided that all NLOS paths arrive from the opposite direction. Fig. 2 shows the maximum AS as a function of the KF for our proposed model. The requested AS was set to 100° . Those values cannot be achieved by the SSF model. However, for NLOS propagation, the achievable azimuth spread converges to values around 80° , and the elevation spread is around 45° . If the requested AS is larger than the maximum AS, the SSF model adjusts the angles in a way that the AS at the output of the model is close to the maximum AS.

This KF-dependency of AS becomes a limiting factor for the ASA in Fig. 3. For NLOS propagation, the output curves start to diverge at around 60° and almost none of the output values exceed 95° . This agrees well with the results in Fig. 2. In the LOS case, the 3GPP-NR model defines an average KF of 9 dB with 5 dB standard deviation (STD) and an ASA of around

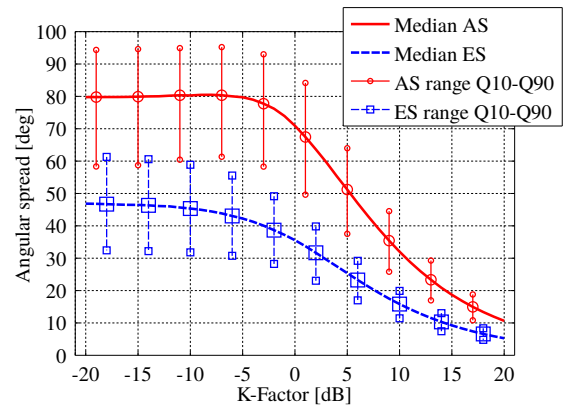


Fig. 2. Maximal Angular Spread vs. K-Factor

50°. This is not achievable even under ideal circumstances. Still, the new SSF model produces ASA of around 30° as predicted by Fig. 2.

Lastly, there are some offsets for the ESD, which is the only parameter which is not frequency-dependent. The 3GPP-NR model requires very low values around 0.6° which depend on the distance between BS and MT. However, the new SSF almost doubles these values and introduces some frequency-dependency for the NLOS scenario. This comes from the application of the LOS angles in Sec. II-d. There is some mixing of the azimuth and elevation characteristics due to the spherical rotations introduced by (25). However, this does not change the capacity of the wireless link since the overall AS does not change.

IV. CONCLUSIONS

The proposed modifications to the 3GPP-NR small-scale-fading (SSF) model enable the simultaneous simulation of wireless channels including spatial consistency, simultaneous mobility of the transmitter and receiver, and the simultaneous simulation of multiple frequencies. This was not possible with the existing 3GPP-NR model which includes spatial consistency and multi-frequency simulations only as optional features and no D2D modeling at all. However, these features are essential for many emerging wireless technologies in the 5G era. Our proposed SSF model includes all these features and seamlessly integrates with the remaining NR model. This has been demonstrated by comparing the output of the new SSF model with the UMi LSF parameter distributions provided by 3GPP. An open-source implementation of our model is provided to the community within QuaDRiGa version 2.2 [4].

ACKNOWLEDGEMENT

The authors thank the Celtic Office and national funding authorities BMBF in Germany, Business Finland, and MINETAD in Spain for supporting this research and development through the ReICOvAir project. The research leading to these results has received funding from the European Union H2020 5GPPP under grant n. 815323 and supported by the Institute for Information & communications Technology Promotion (IITP) grant funded by the Korea government (MSIT) (No.2018-0-00175, 5G AgiLe and fLexible integration of SaTellite And cellularR).

REFERENCES

- [1] 3GPP TR 25.996 v6.1.0, "Spatial channel model for multiple input multiple output (MIMO) simulations," Tech. Rep., 2003.
- [2] 3GPP TR 38.901 v15.0.0, "Study on channel model for frequencies from 0.5 to 100 GHz," Tech. Rep., 2018.
- [3] S. Jaeckel, L. Raschkowski, F. Burkhardt, and L. Thiele, "Efficient sum-of-sinusoids based spatial consistency for the 3gpp new-radio channel model," *Proc. IEEE Globecom Workshops '18*, 2018.
- [4] [Online]. Available: <http://www.quadriga-channel-model.de>
- [5] M. Gudmundson, "Correlation model for shadow fading in mobile radio systems," *IET Electron Lett.*, vol. 27, no. 23, pp. 2145–2146, November 1991.
- [6] M. Peter, R. J. Weiler, F. Undi, F. El-Kanawati, S. Jaeckel, L. Raschkowski, L. Thiele, K. Sakaguchi, and W. Keusgen, "Investigations on the frequency dependence of the delay spread in an UMi street canyon scenario," in *2016 International Symposium on Antennas and Propagation (ISAP)*, Oct 2016, pp. 616–617.

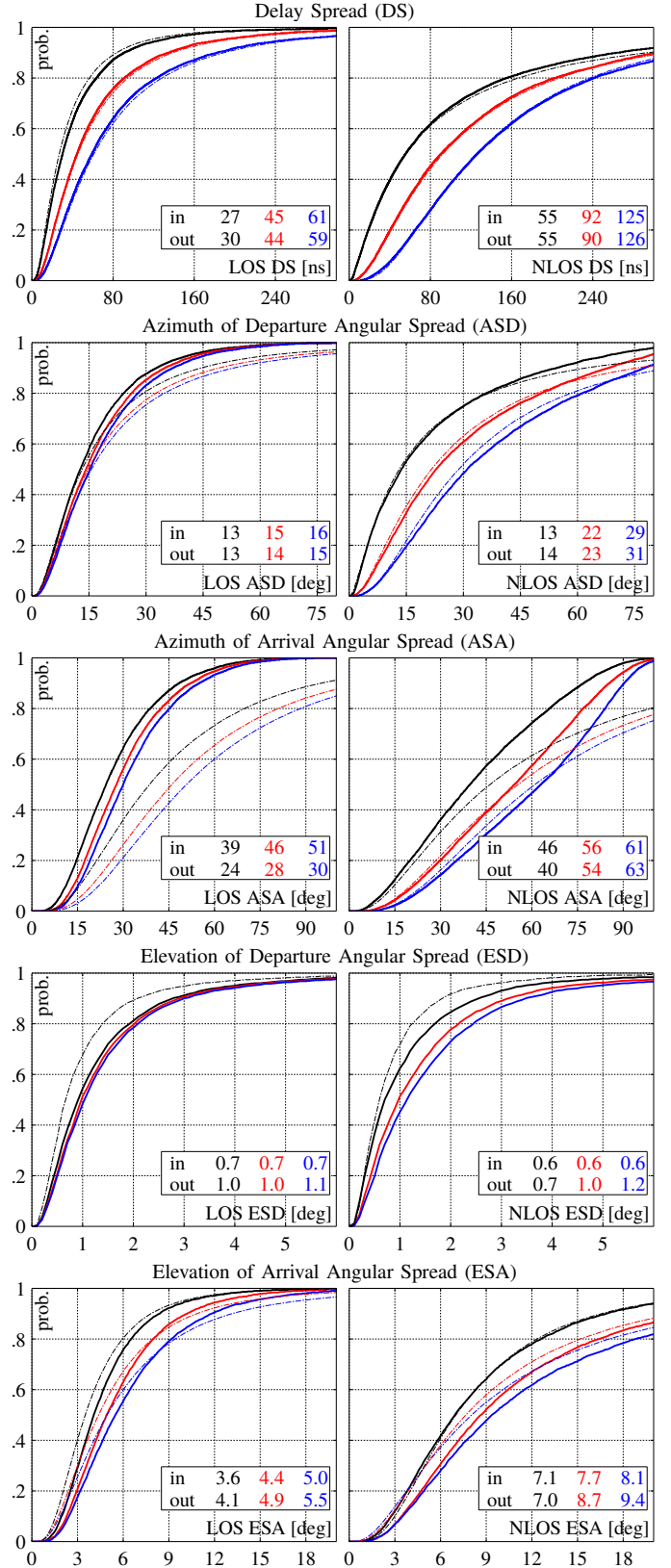


Fig. 3. Simulation Results for the 3GPP-NR UMi Scenario